Pathophysiology 26 (2019) 31–38

Contents lists available at ScienceDirect

Pathophysiology

journal homepage: www.elsevier.com/locate/pathophys

Short- and long-term roles of phosphatidylinositol 4,5-bisphosphate PIP_2 on Cav3.1- and Cav3.2-T-type calcium channel current

Yangong Liu[a,b,1], Tomohiro Iwano[b,1], Fangfang Ma[a,b], Pu Wang[a,b], Yan Wang[b], Mingqi Zheng[a], Gang Liu[a], Katsushige Ono[b,*]

[a] Department of Cardiology, The First Hospital of Hebei Medical University, 89 Donggang Road, Shijiazhuang, Hebei Province, 050031, People's Republic of China
[b] Department of Pathophysiology, Oita University School of Medicine, Yufu, Oita, 879-5593, Japan

ARTICLE INFO

Article history:
Received 1 August 2018
Received in revised form
30 November 2018
Accepted 1 December 2018

Keywords:
Phosphatidylinositol-4
5-bisphosphate (PIP_2)
T-type calcium channel
$Ca_V3.1$
$Ca_V3.2$

ABSTRACT

T-type calcium (Ca^{2+}) channels play important physiological functions in excitable cells including cardiomyocyte. Phosphatidylinositol-4,5-bisphosphate (PIP_2) has recently been reported to modulate various ion channels' function. However the actions of PIP_2 on the T-type Ca^{2+} channel remain unclear. To elucidate possible effects of PIP_2 on the T-type Ca^{2+} channel, we applied patch clamp method to investigate recombinant $Ca_V3.1$- and $Ca_V3.2$-T-type Ca^{2+} channels expressed in mammalian cell lines with PIP_2 in acute- and long-term potentiation. Short- and long-term potentiation of PIP_2 shifted the activation and the steady-state inactivation curve toward the hyperpolarization direction of $Ca_V3.1$-$I_{Ca.T}$ without affecting the maximum inward current density. Short- and long-term potentiation of PIP_2 also shifted the activation curve toward the hyperpolarization direction of $Ca_V3.2$-$I_{Ca.T}$ without affecting the maximum inward current density. Conversely, long-term but not short-term potentiation of PIP_2 shifted the steady-state inactivation curve toward the hyperpolarization direction of $Ca_V3.2$-$I_{Ca.T}$. Long-term but not short-term potentiation of PIP_2 blunted the voltage-dependency of current decay $Ca_V3.1$-$I_{Ca.T}$. PIP_2 modulates $Ca_V3.1$- and $Ca_V3.2$-$I_{Ca.T}$ not by their current density but by their channel gating properties possibly through its membrane-delimited actions.

1. Introduction

Voltage-gated ion channels play major roles in excitable cells by regulating the flow of ions across the plasma membrane in response to changes in membrane potentials. Because voltage-gated ion channels modify cellular metabolic conditions by changing cytoplasmic ionic concentrations and electrical potentials, it is postulated that channels are regulators of cellular metabolic states, and vice versa. Voltage-gated ion channels can be regulated by cellular metabolites including phospholipids. Modulation of ion channels by phospholipids includes phosphatidylinositol 4,5-bisphosphate (PIP_2), an important signaling molecule which is cleaved by phospholipase C (PLC) to inositol 1,4,5-triphosphate (IP_3) and diacylglycerol (DAG) [1]. In cardiomyocytes, IP_3 mobilizes Ca^{2+} from sarcoplasmic reticulum, while DAG activates protein kinase C (PKC). Importantly, PIP_2 itself has a potential to act as a signaling molecule through direct interactions with ion channels [1].

Two types of voltage-gated Ca^{2+} channels are functionally expressed in cardiac myocytes: the L-type Ca^{2+} channels and the T-type Ca^{2+} channels. The L-type Ca^{2+} channels are abundantly expressed and play crucial roles in excitation-contraction (E—C) coupling and electrical conduction in cardiomyocytes. On the other hand, the T-type Ca^{2+} channels are expressed in embryonic and neonatal cardiomyocytes, but are scarcely expressed in adult ventricular myocytes. The strongest evidence of their function is that T-type Ca^{2+}channels participate in pacemaking in the sinoatrial node [2].

We have previously reported that activation of PKC augmented $Ca_V3.2$-T-type Ca^{2+} channel current in heterologous expression system by use of human cardiac $Ca_V3.2$ channels expressed in HEK293 cells [3]. The goal of the present study, in this context, was to use this model and assess the short- and long-term effect of PIP_2 on the Cav3.1- and Cav3.2-T-type Ca^{2+} channel currents ($I_{Ca.T}$).

* Corresponding author at: Department of Pathophysiology, Oita University School of Medicine, 1-1 Idaigaoka, Hasama, Yufu, Oita, 879-5593, Japan.
E-mail address: ono@oita-u.ac.jp (K. Ono).
[1] Yangong Liu and Tomohiro Iwano contributed equally to this work.

https://doi.org/10.1016/j.pathophys.2018.12.001
0928-4680/

2. Materials and methods

2.1. Cav3.1/Cav3.2-HEK293 cells culture

This study was approved by the Animal Use Committee of Oita University School of Medicine. The α1 G subunit ($Ca_V3.1$) and α1H subunit ($Ca_V3.2$) derived from human heart which forms cardiac T-type Ca^{2+} channels were stably expressed in human embryonic kidney (HEK)-293 cells without any auxiliary subunits. A detailed profile and procedure for channel expression were described in a previous report [2]. cDNA encoding the human cardiac α1 G subunit (*CACNA1G*) and α1H subunit (*CACNA1H*) were respectively inserted into the transfection vector pcDNA3, and HEK-293 cells were transfected with 2 μg of this vector using the calcium phosphate precipitation method. Recombinant HEK-293 cells, HEK-$Ca_V3.1$ cells and HEK-$Ca_V3.2$ cells, were maintained in Dulbecco's Modified Eagle Medium (DMEM) supplemented with 10% fetal calf serum, 100 U ml^{-1} penicillin and 100 mg ml^{-1} streptomycin, in an atmosphere of 95% O_2 plus 5% CO_2 at 37°. This medium was supplemented with 300 mg ml^{-1} G418 (neomycin analogue) for the selection of recombinant HEK-293 cells.

2.2. Electrophysiology

Recombinant HEK-$Ca_V3.1$ and HEK-$Ca_V3.2$ cells were seeded onto glass-bottom dishes and incubated in culture medium for 12–48 h before the electrophysiological measurements. Macroscopic T-type Ca^{2+} channel currents ($I_{Ca.T}$) were recorded by whole-cell patch clamp using an EPC-9 amplifier controlled by Pulse ver. 8 software (HEKA Eletronik, Lambrecht, Germany). Patch pipettes were pulled from 75-mm plain capillary tubes (Drummond Scientific Co., Broomall, PA, USA) by Model P-97 (Sutter Instrument Co., Novato, CA, USA), and were heat-polished subsequently to achieve the pipette resistance at 2–4 MΩ when filled with the pipette solution. Series resistance was compensated electrically, as much as possible, without oscillation (60–75%). Capacitance was canceled by the built-in circuitry of the amplifier. Current signals were usually filtered at 2 kHz and digitized at 10 kHz, and stored on a computer. The $I_{Ca.T}$ current was elicited by 200 ms-depolarizing steps from a holding potential of -140 mV to potentials ranging from -120 mV to +50 mV in 5-mV increments. To investigate the channel availability (steady-state inactivation), conventional double-pulse protocol was applied at every 5 s (s): test pulses of 400 ms at -10 mV following prepulses of 1000 ms from -100 to 0 mV (increment = 5 mV) were applied. To examine long-term effects of PIP_2, we cultured HEK-$Ca_V3.1$ cells and HEK-$Ca_V3.2$ cells with or without a PI_3 kinase inhibitor wortmannin in combined with a PLC inhibitor 1-[6-((17β-3-methoxyestra-1,3,5(10)-trien-17-yl)amino)hexyl]-1H-pyrrole-2,5-dione (U73122) for 24 h in glass-bottom dishes, followed by PIP_2-free culture medium (DMEM) for 6 h. Voltage-dependent effects of PIP_2 on $I_{Ca.T}$ were appreciated in the conductance transforms. Relative conductance (activation) values were calculated as follows:

$$Fractional conductance = I_{Ca.T}/G_{max}(V_t\text{-}V_{rev}), \quad (A)$$

where $I_{Ca.T}$ represents the current amplitude at the test potential (V_t) and G_{max} is the maximal conductance value obtained from linear regression line of each I–V relation extrapolated through the estimated reversal potential (V_{rev}). Voltage-dependent activation and availability (steady-state inactivation) were evaluated by a Boltzmann equation fit to the normalized data to peak currents measured in protocols as follows:

$$Fraction = 1/\{1 + \exp[(V\text{-}V_{0.5})/k]\}, \quad (B)$$

where the normalized data (Fraction) were expressed as a function of voltage (V), the test potential in the case of conductance and the conditioning potential in the case of voltage-dependent availability. Parameters estimated by the fit were the half-point of the relationship ($V_{0.5}$) expressed in mV, and *k* is the slope factor. Time constant for the current decay was fitted by a single exponential equation. Voltage dependency of the current decay (time constant) was also assessed by a single exponential equation. All the current measurements were done at room temperature (20–23 °C).

2.3. Solutions and chemicals

The recording chamber was filled with bath solution of the following composition (mM): Tetraethylammonium chloride120, CsCl 6, 4-aminopyridine 5, $MgCl_2$ 0.5, 4, 4′-Diisothiocyanatostilbene- 2, 2′-disulfonic acid disodium salt hydrate 0.5, HEPES 10, $CaCl_2$ 1.8, and glucose 10 (pH was adjusted to 7.4 with 1 N Tetraethylammonium hydroxide solution). The patch-clamp electrode was filled with pipette solution of (mM): CsCl 130, $MgCl_2$ 2, Adenosine 5′-Triphosphate 2, Guanosine 5′-Triphosphate 0.5, EGTA 5, and HEPES 5 (pH was adjusted to 7.3 with 1 N CsOH). Data were acquired by using computer software (Pulse/PulseFit, V. 8.11, HEKA Electronik, Lambrecht, Germany), and all curve fittings and figures were made on SigmaPlot (version 10; SPSS, Inc., Chicago, IL, USA).

2.4. Drugs and chemicals

Accumulation or activation of phosphatidylinositol 4,5-bisphosphate (PIP_2) at plasma membrane was obtained by an application of an inhibitor of PLC (U73122) in combined with a phosphoinositide 3-kinase (PI_3) kinase inhibitor (wortmannin). These reagents were dissolved in the bath solution (short-term effect study) or in the culture medium DMEM without fetal calf serum (long-term effect study) stored frozen, and dissolved immediately before the experiments to obtain the final concentration of 10 μM (U73122) and 10 nM (wortmannin), respectively. All chemicals and pharmacological reagents were purchased from Wako Pure Chemical Ind. (Osaka, Japan).

2.5. Statistical analyses

Group data show as mean ± standard deviation (SD). Paired- (short-term effect study) and non-paired (long-term effect study) student's *t*-test was used for comparison between two means. Differences were considered significant when p value were<0.05.

3. Results

3.1. Short-term effects of PIP_2 on Cav3.1- and Cav3.2-channel currents

In the first series of experiments we investigated the possible short-term (5 min) effects of PIP_2 on the T-type Ca^{2+} channel currents ($I_{Ca.T}$); $Ca_V3.1$- and $Ca_V3.2$-T-type Ca^{2+} channel current ($I_{Ca.T}$). Because blocking of phosphoinositide-3 kinase (PI_3 kinase) and/or phospholipase C (PLC) causes an increase of PIP_2 as often described in the literatures [1], we examined effects of a PI_3 kinase inhibitor wortmannin in combined with a PLC inhibitor U73122 on $I_{Ca.T}$ to assess the short-term effects of PIP_2 in this heterologous expression system. Fig. 1A illustrates typical acute effects of PIP_2 activation or potentiation on $Ca_V3.1$-$I_{Ca.T}$ current family, and Fig. 1B for the current (I)-voltage (V) relationships. Fig. 1C illustrates typical acute effects of PIP_2 activation on $Ca_V3.2$-$I_{Ca.T}$ current family, and Fig. 1D for the I–V relationships. Activation of PIP_2 exerted no effect on the maximum peak current of $Ca_V3.1$-$I_{Ca.T}$ (Fig. 1B, E) and

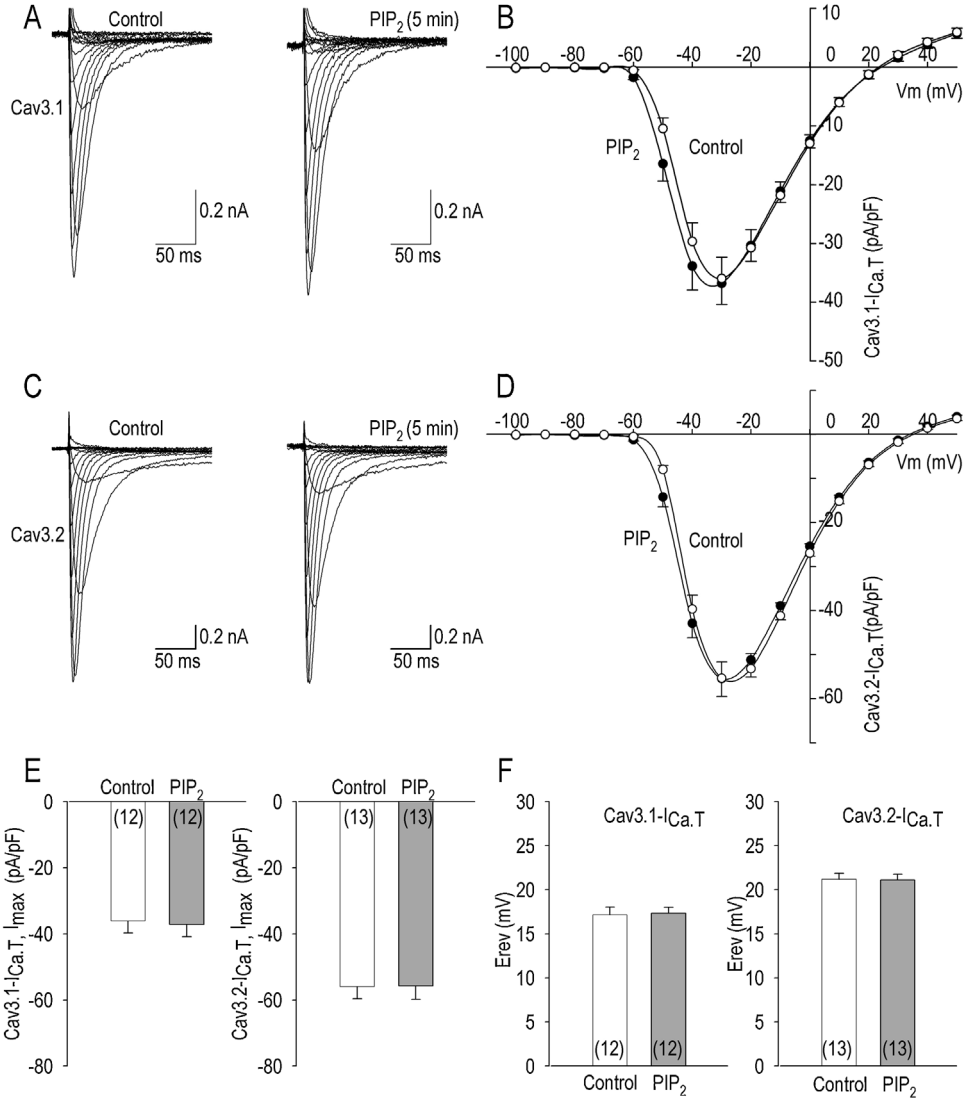

Fig. 1. Short-term effects of PIP_2 activation on $Ca_V3.1$- and $Ca_V3.2$-$I_{Ca.T}$. A, B. Representative whole cell current families in control and after activation of PIP_2 in 5 min obtained from an HEK-$Ca_V3.1$ cell (A), and their current-voltage (I–V) relationship with (●) or without PIP_2 activation (○, n = 12) (B). C, D. Representative whole cell current families in control and after activation of PIP_2 in 5 min obtained from an HEK-$Ca_V3.2$ cell (C), and their current-voltage (I–V) relationship with (●) or without PIP_2 activation (○, n = 13) (D). E. Changes of the maximum $Ca_V3.1$-$I_{Ca.T}$ (left) and $Ca_V3.2$-$I_{Ca.T}$ (right) with or without PIP_2 activation. F. Changes of reversal potentials (Erev) of $Ca_V3.1$-$I_{Ca.T}$ (left) and $Ca_V3.2$-$I_{Ca.T}$ (right) with or without PIP_2 activation. Erev was calculated by the currents at the potentials of the maximum conductance (from -20 mV to +10 mV). Though the protocol, $I_{Ca.T}$ was elicited from the holding potential of -100 mV at the test potentials (from -100 mV to +50 mV) with the stimulation frequency of 0.5 Hz.

$Ca_V3.2$-$I_{Ca.T}$ (Fig. 1D, E). Also the reversal potentials of $Ca_V3.1$- and $Ca_V3.2$-$I_{Ca.T}$ were unaffected by an acute activation of PIP_2.

Steady-state inactivation kinetics were studied with or without activation of PIP_2. We measured the channel availability or the steady-state inactivation property by applying a 1000-ms prepulse of various potentials prior to a test pulse at 0 mV. Fig. 2 illustrates the activation and steady-state inactivation curves of Cav3.1- and Cav3.2-$I_{Ca.T}$ with or without PIP_2 activation. The averaged data points for activation curves could be fitted by a single Boltzmann equation with the parameter values of $V_{0.5}$ = -42.7 ± 3.2 mV and k = -4.5 mV for control, and $V_{0.5}$ = -45.3 ± 3.5 mV and k = -4.5 mV for PIP_2 in $Ca_V3.1$-$I_{Ca.T}$, where $V_{0.5}$ = -39.3 ± 2.2 mV and k = -5.1 mV for control, and $V_{0.5}$ = -41.4 ± 2.6 mV and k = -5.2 mV for PIP_2 in $Ca_V3.2$-$I_{Ca.T}$. The averaged experimental points for steady-state inactivation curves were fitted by a Boltzmann equation with values of $V_{0.5}$ = -62.1 ± 1.9 mV and k = 4.4 mV for control, and $V_{0.5}$ = -65.3 ± 2.7 mV and k = 4.6 mV for PIP_2 in $Ca_V3.1$-$I_{Ca.T}$, where $V_{0.5}$ = -53.1 ± 1.2 mV and k = 4.0 mV for control, and $V_{0.5}$ = -53.3 ± 1.4 mV and k = 4.0 mV for PIP_2 in $Ca_V3.2$-$I_{Ca.T}$ (Fig. 2). Short-term activation of PIP_2 significantly shifted the activation and the steady-state inactivation curve toward the hyperpolarization direction of $Ca_V3.1$-$I_{Ca.T}$, whereas short-term potentiation of PIP_2 shifted the activation but not the steady-state inactivation curve toward the hyperpolarization direction of $Ca_V3.2$-$I_{Ca.T}$.

3.2. *Long-term effects of PIP_2 on Cav3.1- and Cav3.2-channel currents*

The above results indicate that activation of PIP_2 modifies $I_{Ca.T}$ gating properties as a short-term signal regulator. Therefore we then investigated the role of prolonged activation of PIP_2 on the $I_{Ca.T}$ by applying a PI_3 kinase inhibitor wortmannin in combined with a PLC inhibitor U73122 into the culture medium for 24 h. Prolonged activation of PIP_2 was without effect on the maximum peak currents of $Ca_V3.1$-$I_{Ca.T}$ and $Ca_V3.2$-$I_{Ca.T}$, in the manner similar to those of the short-term effect (Fig. 3). Moreover, prolonged activation of PIP_2 shifted the activation and the steady-state inactivation curves of both $Ca_V3.1$-$I_{Ca.T}$ and $Ca_V3.2$-$I_{Ca.T}$ toward the depolarized

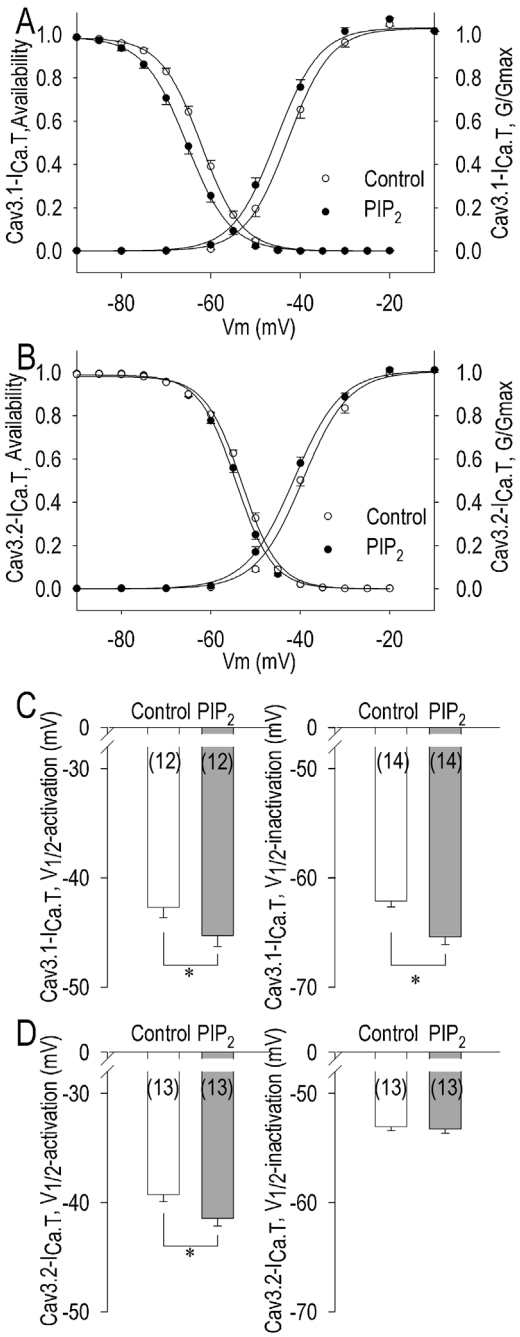

Fig. 2. Voltage dependence of steady-state inactivation and activation for $Ca_V3.1$- and $Ca_V3.2$-$I_{Ca.T}$, and their modification by short-term activation of PIP_2. A, B. The activation and steady-state inactivation curves for $Ca_V3.1$-$I_{Ca.T}$ with (●) or without (○) PIP_2 activation for 5 min (A), and for $Ca_V3.2$-$I_{Ca.T}$ with (●) or without (○) PIP_2 activation for 5 min (B). The activation parameter, or chord conductance (G), was calculated by dividing the peak current measured for each test potential by the driving force. Steady-state inactivation was assessed by measuring the channel availability or the proportional peak current at 0 mV after a 500 ms-long prepulse for various potentials. Smooth solid curves represent Boltzmann fits to the data, yielding half-maximal activation ($V_{0.5}$-activation) and half-maximal inactivation potentials ($V_{0.5}$-inactivation). C. $V_{0.5}$-activation and $V_{0.5}$-inactivation for $Ca_V3.1$-$I_{Ca.T}$ with or without PIP_2 activation. D. $V_{0.5}$-activation and $V_{0.5}$-inactivation for $Ca_V3.2$-$I_{Ca.T}$ with or without PIP_2 activation.

potentials with similarity to the short-term effect of PIP_2 (Fig. 4). The averaged data points for activation curves could be fitted by a single Boltzmann equation with the parameter values of $V_{0.5}$ = -40.2 ± 3.1 mV and k = -5.0 mV for control, and $V_{0.5}$ = -43.3 ± 3.2 mV and k = -5.5 mV for PIP_2 in $Ca_V3.1$-$I_{Ca.T}$, where $V_{0.5}$ = -36.6 ± 3.1 mV and k = -5.6 mV for control, and $V_{0.5}$ = -38.1 ± 2.5 mV and k = -5.4 mV for PIP_2 in $Ca_V3.2$-$I_{Ca.T}$. The averaged experimental points for steady-state inactivation curves were fitted by a Boltzmann equation with values of $V_{0.5}$ = -61.7 ± 2.6 mV and k = 4.2 mV for control, and $V_{0.5}$ = -63.9 ± 3.0 mV and k = 4.1 mV for PIP_2 in $Ca_V3.1$-$I_{Ca.T}$, where $V_{0.5}$ = -53.7 ± 1.8 mV and k = 3.9 mV for control, and $V_{0.5}$ = -54.7 ± 1.6 mV and k = 4.0 mV for PIP_2 in $Ca_V3.2$-$I_{Ca.T}$ (Fig. 4). Shifts of the activation curves toward the hyperpolarization direction of these two isoforms of $I_{Ca.T}$ were nearly equal in spite of the difference of molecular structures.

3.3. Fast inactivation or current decays and their voltage dependency

The inactivation kinetics of the channel were further studied by using a depolarization pulse of 250 ms from -100 to +120 mV in 10 mV steps driven from a holding potential of -100 mV. To explore the changes of current decays and their dependency on the voltage, current decays were fitted by a single exponential function, and the time constants were plotted against the test potentials (Fig. 5). Time constants (τ, Tau) were strongly dependent on the voltage in the range of -50 to +10 mV. The voltage dependency of Tau or voltage constant was unaffected by an acute activation of PIP_2 (Fig. 5C). On the other hand, long-term activation of PIP_2 blunted the voltage dependency of Tau in $Ca_V3.1$-$I_{Ca.T}$ but not in $Ca_V3.2$-$I_{Ca.T}$ (Fig. 6C), as reflected by a large change of $V_{0.5}$-activation of $Ca_V3.1$ (+3.1 mV) than that of $Ca_V3.2$ (+1.5 mV) in Fig. 4.

4. Discussion

The present study demonstrates that acute activation of PIP_2 modifies the gating of Cav3.1- and Cav3.2-T-type Ca^{2+} channels in heterologously expressed HEK-293 cells. Specifically, the activation curves of $Ca_V3.1$- and $Ca_V3.2$-$I_{Ca.T}$ and the steady-state inactivation curve of $Ca_V3.1$-$I_{Ca.T}$ were shifted toward the hyperpolarized direction by PIP_2. More importantly, prolonged activation of PIP_2 (24 h) did not further modify the gating of the both currents (except the small but significant shift of the steady-state inactivation curve of the $Ca_V3.2$-$I_{Ca.T}$ toward the hyperpolarization direction) nor the maximum amplitude of the currents. Conversely, prolonged but not acute activation of PIP_2 blunted the voltage dependency of current decay (fast inactivation) of $Ca_V3.1$- $I_{Ca.T}$.

PIP_2 plays important roles in a wide variety of cellular processes, such as generation of the second messengers DAG and $InsP_3$, regulation of both endocytosis and exocytosis, formation of microvilli, and membrane attachment to the cytoskeleton [4]. Importantly, it has also been appreciated that PIP_2 itself directly controls the function of a variety of channels and transporters either by causing activation—as in the case of inwardly rectifying potassium (Kir) channels [5], the Na^+/Ca^{2+} antiporter [6], the Na^+/H^+ exchanger [7], the TRPM7 channels [8], and the epithelial Na^+ channel (ENaC) [9,10] —or inhibition of ionic transport, such as for TRP-L channels [11], the TRP-V capsaicin receptor [12], the $InsP_3R$ [13], and mammalian rod cyclic nucleotide-gated channels [14], although long-term effects of PIP_2 as a transcription modulator of ion channels are largely unknown. However, no functional description of the T-type Ca^{2+} channel current kinetics by PIP_2 is available. To address this question we intended to clarify the role of PIP_2 on $Ca_V3.1$- and Ca_V-3.2-$I_{Ca.T}$ in heterologously expressed HEK-293 cells. It is widely accepted that PIP_2 is generated by phosphorylation of PI3P, PI4P or PI5P by PIP kinases, PIPKI or PIPKII. Because, to the best of our knowledge, these kinds of enzymes have not been described in extracellular surface of plasma membrane, changes in intracellular PIP_2 levels might be important for the regulation of channel kinetics in general. Because intracellular application of PIP_2 may interfere

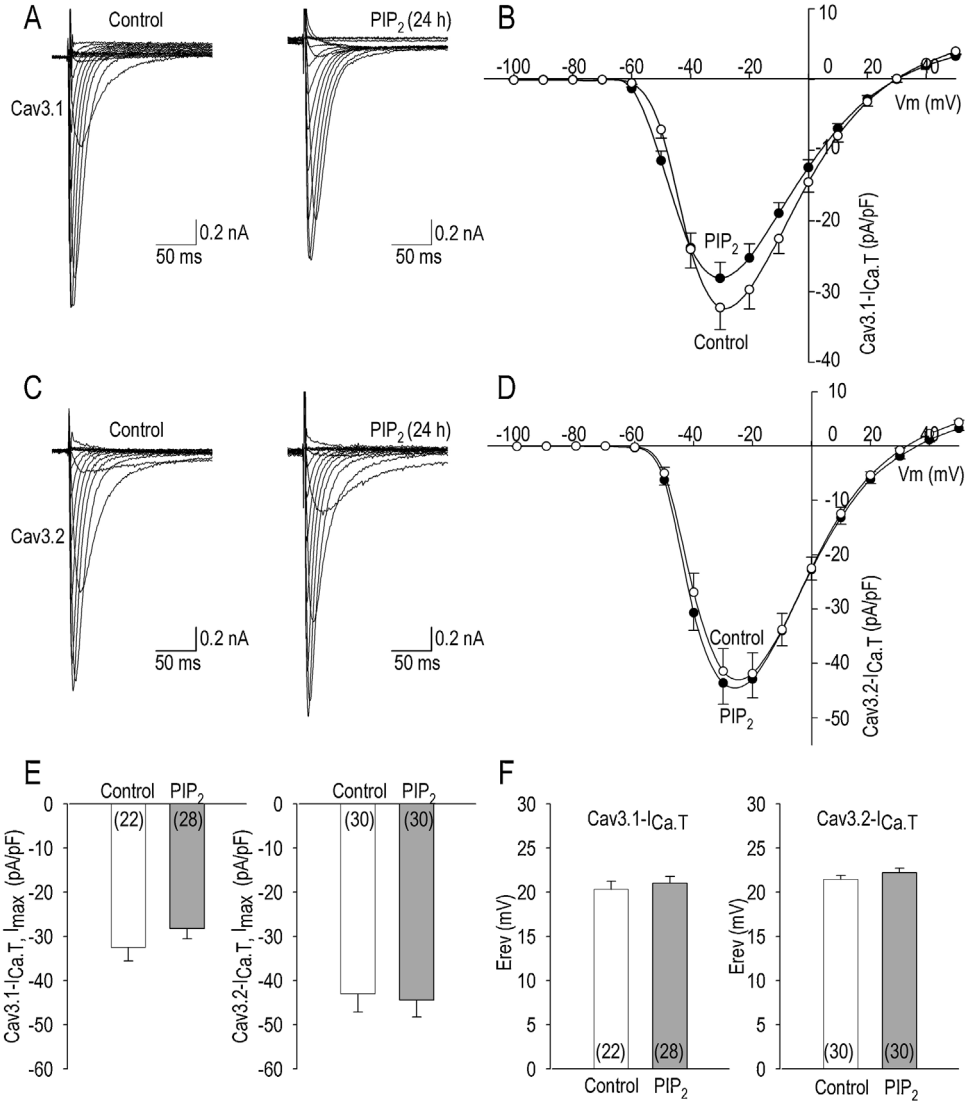

Fig. 3. Long-term effect of PIP_2 activation on $Ca_V3.1$- and $Ca_V3.2$-$I_{Ca.T}$. A, B. Representative whole cell current families in control (vehicle) and after activation of PIP_2 for 24 h obtained from an HEK-$Ca_V3.1$ cell (A), and their current-voltage (I–V) relationship with (●, n = 28) or without PIP_2 activation (○, n = 22) (B). C, D. Representative whole cell current families in control and after activation of PIP_2 for 24 h obtained from an HEK-$Ca_V3.2$ cell (C), and their current-voltage (I–V) relationship with (●, n = 30) or without PIP_2 activation (○, n = 30) (D). E. Changes of the maximum $Ca_V3.1$-$I_{Ca.T}$ (left) and $Ca_V3.2$-$I_{Ca.T}$ (right) with or without PIP_2 activation. F. Changes of reversal potentials (Erev) of $Ca_V3.1$-$I_{Ca.T}$ (left) and $Ca_V3.2$-$I_{Ca.T}$ (right) with or without PIP_2 activation. In control condition, a small aliquot of serum-free DMEM solution (~0.1 μL) was applied to the culture medium for 24 h as vehicle. Erev was calculated as described in the figure legend 1.

with cellular physiological metabolic conditions, a direct application of PIP_2 to assess the long-term action may not be suitable in this experimental model. In this context, we employed a standard method to accumulate PIP_2 in the plasma membrane by inhibition of PI3K-mediated and PLC-medicated hydrolysis. It has been previously shown that wortmannin at nanomolar concentrations blocks specifically PI_3 kinases, but at micromolar concentrations it also blocks the activity of most PI4 kinases [15]. Since the PI4 kinases are required for synthesis of the major phospholipid of the plasma membrane, $PI(4,5)P_2$, inhibition of their activity is expected to interfere with replenishment of PIP_2 levels. Since an inhibition of PLC leads to PIP_2 accumulation in plasma membrane, a PLC inhibitor U73122 was employed in combined with wortmannin to accumulate and activate action of PIP_2 in this study, although quantitative assay of PIP_2 accumulation in the plasma membrane was unavailable.

An emerging literature suggests that PIP_2 controls the activity of voltage-gated Ca^{2+} channels. The first study on the voltage-gated Ca^{2+} channel modulation by PIP_2 described that this phosphoinositide shifts the voltage-dependence of activation of the P/Q-type Ca^{2+} channel ($Ca_V2.1$) current toward depolarized potentials [16], which is in sharp contrast to our results on $I_{Ca.T}$. Of note, the Cav2 subfamily (N-and P/Q-type Ca^{2+} channels) are regulated by G protein coupled receptors via a pathway that stimulate $G_{q/11}$ protein to activate PLC, which hydrolyzes PIP_2 to inositol triphosphate (IP_3) and diacylglycerol (GAG) [17–19]. Activation of $G_{q/11}$-coupled receptor has a strong inhibitory effect on $Ca_V3.3$-T-type Ca^{2+} channel, however, on the contrary, the same stimulation causes either no effects or a moderate stimulating effect on $Ca_V3.1$ and $Ca_V3.2$ peak current amplitudes [20]. In accordance with distinct modulation pathways, in the $Ca_V2.2$-*N*-type Ca^{2+} channel in sympathetic neurons, the current inhibition by muscarinic M1 receptor activation was diminished by intracellular application of diC8-PIP_2, and the current recovery was abolished when PIP_2 synthesis was blocked [21]. Because stimulation of $G_{q/11}$-coupled receptors possibly activates phospholipase A2 with the subsequent production of arachidonic acids, these signal molecules could be proposed as the key mediators of Ca_V2 channel modulation [22], which may lead

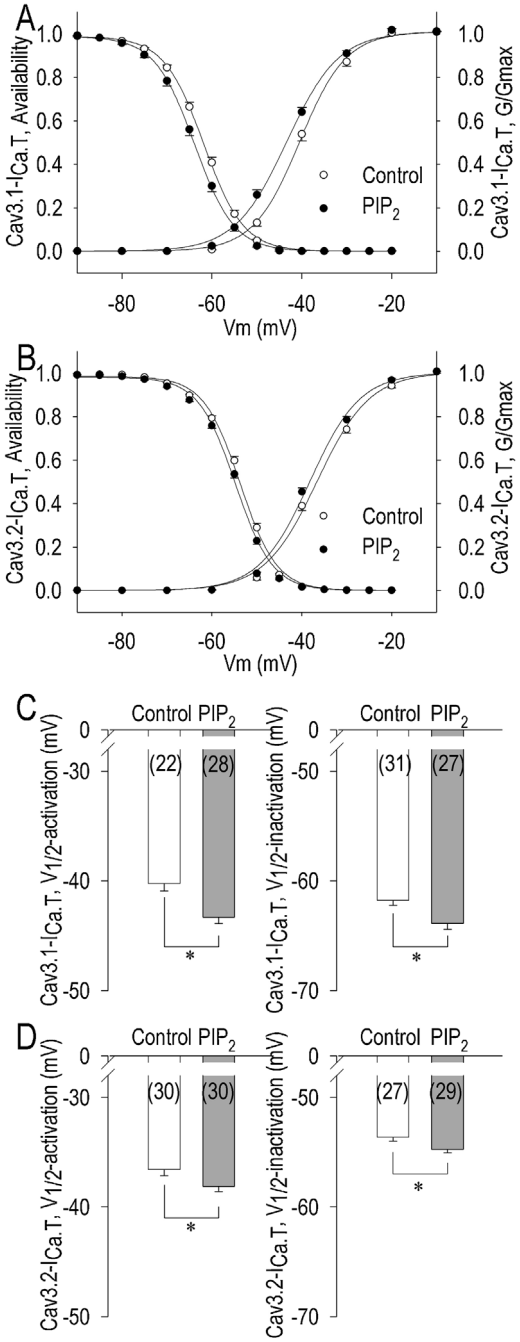

Fig. 4. Voltage dependence of steady-state inactivation and activation for $Ca_V3.1$- and $Ca_V3.2$-$I_{Ca.T}$, and their modification by long-term (24 h) activation of PIP_2. A, B. The activation and steady-state inactivation curves for $Ca_V3.1$-$I_{Ca.T}$ with (●, n = 27–28) or without (○, n = 22–31) PIP_2 activation for 24 h (A), and for $Ca_V3.2$-$I_{Ca.T}$ with (●, n = 29–30) or without (○, n = 27–30) PIP_2 activation for 24 h (B). The activation parameter, or chord conductance (G), and the steady-state inactivation parameters were calculated by a method described in the figure legend 2. Smooth solid curves represent Boltzmann fits to the data, yielding half-maximal activation ($V_{0.5}$-activation) and half-maximal inactivation potentials ($V_{0.5}$-inactivation). C. $V_{0.5}$-activation and $V_{0.5}$-inactivation for $Ca_V3.1$-$I_{Ca.T}$ with or without PIP_2 activation for 24 h. D. $V_{0.5}$-activation and $V_{0.5}$-inactivation for $Ca_V3.2$-$I_{Ca.T}$ with or without PIP_2 activation for 24 h. In control condition, a small aliquot of serum-free DMEM solution (~0.1 μL) was applied to the culture medium for 24 h as vehicle.

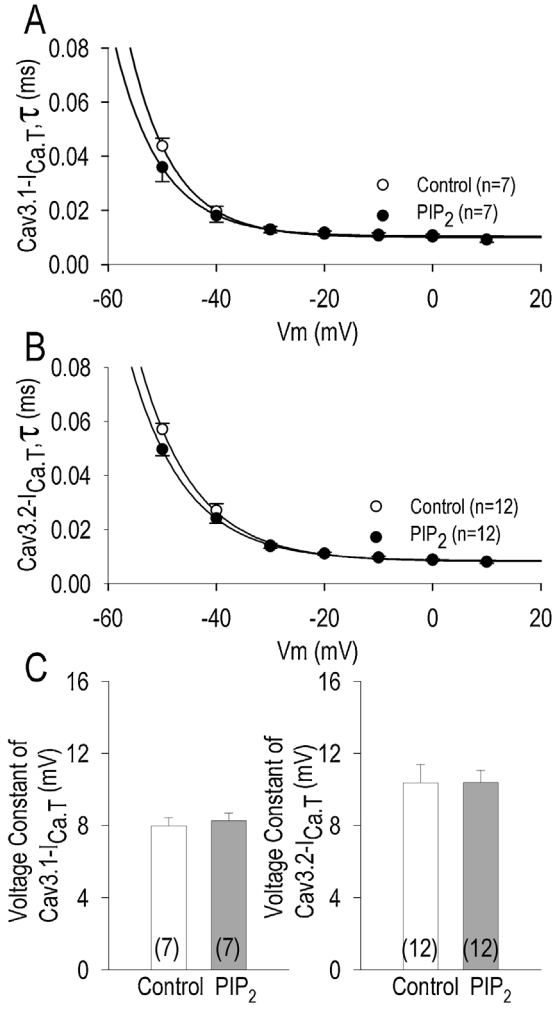

Fig. 5. Time constants for fast inactivation (current decay or relation) for $Ca_V3.1$- and $Ca_V3.2$-$I_{Ca.T}$, and their modification by short-term (5 min) activation of PIP_2. A. The decay of the $Ca_V3.1$-$I_{Ca.T}$ with (●, n = 7) or without PIP_2 activation (○, n = 7) was fitted by a single exponential, yielding inactivation time constants (tau, τ) at the respective test potentials (abscissa). Smooth solid curves represent a single exponential fits to the data, yielding voltage dependency of the $Ca_V3.1$-$I_{Ca.T}$ decay with or without PIP_2 activation. B. The decay of the $Ca_V3.2$-$I_{Ca.T}$ with (●, n = 12) or without PIP_2 activation (○, n = 12) was fitted by a single exponential, yielding inactivation time constants (tau, τ) at the respective test potentials (abscissa). Smooth solid curves represent a single exponential fits to the data, yielding voltage dependency of the $Ca_V3.2$-$I_{Ca.T}$ decay with or without PIP_2 activation. C. Dependency of time constant for fast inactivation on membrane potentials, namely voltage constant, was plotted with or without PIP_2 activation based on panels A and B.

to the differential modulation of the voltage-gated Ca^{2+} channel currents by PIP_2.

The second goal of this study was to identify the long-term action of PIP_2 for the T-type Ca^{2+} channel expression. The long-term effects of PIP_2 activation on the maximum peak current and the kinetics of $Ca_V3.1$- and $Ca_V3.1$- $I_{Ca.T}$ were nearly identical to those of the short-term effects, it is suggested that PIP_2 does not act as a molecule to modify transcription/translation of the Cav3.1- and Cav3.2-T-type Ca^{2+} channels. Also accumulation of PIP_2 in the plasma membrane may not interfere with the trafficking of the channels to the cellular membrane. Although sequence identity across the Ca_V3 family is approximately 40% per cent (e.g. comparing $Ca_V3.1$ and $Ca_V3.2$), the highest level of conservation is found in the membrane spanning region [23], which is probably responsible for the similarity of PIP_2 effects on the channel kinetics between these two isoforms. Despite our efforts to identify the short- and long-tern effects of PIP_2 on $Ca_V3.1$ and $Ca_V3.2$ channels, no mechanistic insight on the PIP_2 effects were gleaned in this study. Voltage-gated Ca^{2+} channels usually need auxiliary subunits for proper trafficking to the plasma membrane and the channel gating. Especially β subunit plays crucial roles in the surface expression of the Ca^{2+} channels and fine-tuning of channel

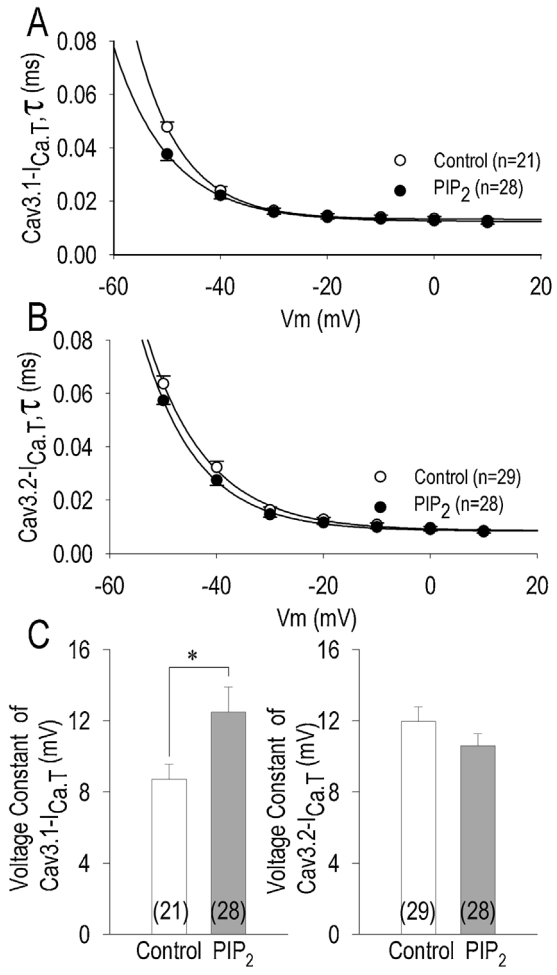

Fig. 6. Time constants for fast inactivation (current decay or relation) for $Ca_V3.1$- and $Ca_V3.2$-$I_{Ca.T}$, and their modification by long-term (24 h) activation of PIP_2. A. The decay of the $Ca_V3.1$-$I_{Ca.T}$ with (●, n = 28) or without PIP_2 activation (○, n = 21) was fitted by a single exponential, yielding inactivation time constants (tau, τ) at the respective test potentials (abscissa). Smooth solid curves represent a single exponential fits to the data, yielding voltage dependency of the $Ca_V3.1$-$I_{Ca.T}$ decay with or without PIP_2 activation. B. The decay of the $Ca_V3.2$-$I_{Ca.T}$ with (●, n = 28) or without PIP_2 activation (○, n = 29) was fitted by a single exponential, yielding inactivation time constants (tau, τ) at the respective test potentials (abscissa). Smooth solid curves represent a single exponential fits to the data, yielding voltage dependency of the $Ca_V3.2$-$I_{Ca.T}$ decay with or without PIP_2 activation. C. Dependency of time constant for fast inactivation on membrane potentials, namely voltage constant, was plotted with or without PIP_2 activation based on panels A and B.

gating. Although this study demonstrates that $Ca_V3.1$ and $Ca_V3.2$ channels are modulated by PIP_2, binding sites and/or molecular mechanism of PIP_2 regulation remains unclear. It was recently reported that subcellular localization of β subunit is a key factor for the control of PIP_2 sensitivity of the voltage-gated Ca^{2+} channels [24]. Nevertheless this mechanism may not be responsible the $Ca_V3.1$- and $Ca_V3.2$-T-type Ca^{2+} channels because the β subunit is absent from T-type Ca^{2+} channels, and the channels are made up of only an α1 subunit [23]. According to the previous studies of the β subunit function, polybasic motif at the C-terminal end of the I-II linker of Ca_V3 channels is suggested as a potential PIP_2 interaction site, although additional experiments are definitely needed. Pathological significance of the modulation of gating properties of Cav3 channels by PIP_2 may include a regulation of cardiac excitability or automaticity. Although the amplitude of $I_{Ca.T}$ window current was unchanged by PIP_2 activation, the window current increased in the range of potentials in hyperpolarization direction, which would increase the membrane potentials at which the depolarization would occur [25]. In spite of the their rapid kinetics of inactivation, the existence and the shift of their voltage range toward the hyperpolarization by PIP_2 activation would confer a role of the T-type Ca^{2+} channels in acceleration of heart rhythm in the heart responding to a change in local phosphoinositides signal in the plasma membrane.

5. Conclusions

Our present findings demonstrate that PIP_2 modulates $Ca_V3.1$- and $Ca_V3.2$-$I_{Ca.T}$ not by their current density but by their channel gating properties possibly through its membrane-delimited actions. Although a requirement of PIP_2 is not clearly established yet for $Ca_V3.1$- and $Ca_V3.2$-$I_{Ca.T}$, this study revealed that T-type Ca^{2+} channel gating properties, at least in part, depend on actions of phosphoinositides of plasma cell membranes.

Acknowledgements and Research Support

This study was supported in part by Grants-in-aid for Scientific Research from the Ministry of Education, Culture, Sports, Science and Technology of Japan (KAKEN, No. 25460292) to K.O.

References

[1] C.A. Barlow, R.S. Laishram, R.A. Anderson, Nuclear phosphoinositides: a signaling enigma wrapped in a compartmental conundrum, Trends Cell Biol. 20 (2010) 25–35.
[2] L.L. Cribbs, J.H. Lee, J. Yang, J. Satin, Y. Zhang, A. Daud, J. Barclay, M.P. Williamson, M. Fox, M. Rees, E. Perez-Reyes, Cloning and characterization of α1H from human heart, a member of the T-type Ca^{2+} channel gene family, Circ. Res. 83 (1998) 103–109.
[3] Y. Wang, M. Morishima, M. Zheng, T. Uchino, K. Mannen, A. Takahashi, Y. Nakaya, I. Komuro, K. Ono, Transcription factors Csx/Nkx2.5 and GATA4 distinctly regulate expression of Ca^{2+} channels in neonatal rat heart, J. Mol. Cell. Cardiol. 42 (2007) 1045–1053.
[4] M.P. Czech, PIP2 and PIP3: complex roles at the cell surface, Cell 100 (2000) 603–606.
[5] H. Zhang, C. He, X. Yan, T. Mirshahi, D.E. Logothetis, Activation of inwardly rectifying K^+ channels by distinct PtdIns(4,5)P_2 interactions, Nat. Cell Biol. 1 (1999) 183–188.
[6] D.W. Hilgemann, R. Ball, Regulation of cardiac Na^+, Ca^{2+} exchange and K_{ATP} potassium channels by PIP_2, Science 273 (1996) 956–959.
[7] O. Aharonovitz, H.C. Zaun, T. Balla, J.D. Yok, J. Orlowski, S. Grinstein, Intracellular pH regulation by Na^+/H^+ exchange requires phosphatidylinositol 4,5-bisphosphate, J. Cell Biol. 150 (2000) 213–224.
[8] L.W. Runnels, L. Yue, D.E. Clapham, The TRPM7 channel is inactivated by PIP_2 hydrolysis, Nat. Cell Biol. 4 (2002) 329–336.
[9] H.P. Ma, S. Saxena, D.G. Warnock, Anionic phospholipids regulate native and expressed epithelial sodium channel (ENaC), J. Biol. Chem. 277 (2002), 7641-1.
[10] G. Yue, B. Malik, G. Yue, D.C. Eaton, Phosphatidylinositol 4,5-bisphosphate (PIP_2) stimulates epithelial sodium channel activity in A6 cells, J. Biol. Chem. 277 (2002) 11965–11969.
[11] M. Estacion, W.G. Sinkins, W.P. Schilling, Regulation of Drosophila transient receptor potential-like (TrpL) channels by phospholipase C-dependent mechanisms, J. Physiol. 530 (2001) 1–19.
[12] H.H. Chuang, E.D. Prescott, H. Kong, S. Shields, S.E. Jordt, A.I. Basbaum, M.V. Chao, D. Julius, Bradykinin and nerve growth factor release the capsaicin receptor from PtdIns(4,5)P_2-mediated inhibition, Nature 411 (2001) 957–962.
[13] V.D. Lupu, E. Kaznacheyeva, U.M. Krishna, J.R. Falck, I. Bezprozvanny, Functional coupling of phosphatidylinositol 4,5-bisphosphate to inositol 1,4,5-trisphosphate receptor, J. Biol. Chem. 273 (1998) 14067–14070.
[14] K.B. Womack, S.E. Gordon, F. He, T.G. Wensel, C.C. Lu, D.W. Hilgemann, Do phosphatidylinositides modulate vertebrate phototransduction? J. Neurosci. 15 (2000) 2792–2799.
[15] H. Nakanishi, K.A. Brewer, J.H. Exton, Activation of the ζ isozyme of protein kinase C by phosphatidylinositol 3,4,5-trisphosphate, J. Biol. Chem. 20 (1993) 13–16.
[16] L. Wu, C.S. Bauer, X.G. Zhen, C. Xie, J. Yang, Dual regulation of voltage-gated calcium channels by PtdIns(4,5)P_2, Nature 419 (2002) 947–952.
[17] L. Bernheim, D.J. Beech, B. Hille, A diffusible second messenger mediates one of the pathways coupling receptors to calcium channels in rat sympathetic neurons, Neuron 6 (1991) 859–867.
[18] M.L. Brown, G.B. Brown, W.J. Brouillette, Effects of log P and phenyl ring conformation on the binding of 5-phenylhydantoins to the voltage-dependent sodium channel, J. Med. Chem. 40 (1997) 602–607.

[19] D.R. Brown, J.W. Herms, B. Schmidt, H.A. Kretzschmar, PrP and β-amyloid fragments activate different neurotoxic mechanisms in cultured mouse cells, Eur. J. Neurosci. 9 (1997) 1162–1169.
[20] M.E. Hildebrand, L.S. David, J. Hamid, K. Mulatz, E. Garcia, G.W. Zamponi, T.P. Snutch, Selective inhibition of Cav3.3 T-type calcium channels by $G\alpha_{q/11}$-coupled muscarinic acetylcholine receptors, J. Biol. Chem. 282 (2007) 21043–21055.
[21] N. Gamper, V. Reznikov, Y. Yamada, J. Yang, M.S. Shapiro, Phosphatidylinositol 4,5-bisphosphate signals underlie receptor-specific $G_{q/11}$-mediated modulation of N-type Ca^{2+} channels, J. Neurosci. 24 (2004) 10980–10992.
[22] M.L. Roberts-Crowley, T. Mitra-Ganguli, L. Liu, A.R. Rittenhouse, Regulation of voltage-gated Ca^{2+} channels by lipids, Cell Calcium 45 (2009) 589–601.
[23] E. Perez-Reyes, Molecular physiology of low-voltage-activated T-type calcium channels, Physiol. Rev. 83 (2003) 117–161.
[24] C.G. Park, B.C. Suh, The HOOK region of β subunits controls gating of voltage-gated Ca^{2+} channels by electrostatically interacting with plasma membrane, Channels 11 (2017) 467–475.
[25] G.W. Zamponi, Voltage-Gated Calcium Channels: Molecular Biology Intelligence Unit. Landes Bioscience Georgetown, Kluwer Academic, New York, 2005, Chapter 20, Calcium Channels in the Heart 309-319.